NanoAnalysis
An International Journal
Available online at: www.jnanoanalysis.net or www.jnanoanalysis.com

Removal of Cd^{2+} and Zn^{2+} from industrial wastes using novel magnetic N^2,N^6-di(thiazol-2-yl)pyridine-2,6-dicarboxamide nanoadsorbent

Kiomars Zargoosh*, Mohammad Rasoul Sohrabi, Amir Abdolmaleki and Kourosh Firouz

Department of Chemistry, Isfahan University of Technology, Isfahan 84156-83111, Iran

Abstract

In this work N^2,N^6-di(thiazol-2-yl)pyridine-2,6-dicarboxamide (DPD), was synthesized via reaction of 2-aminothiazole and 2,6- pyridinedicarboxylic acid in n-methylpyrrolidine. The obtained (DPD) was characterized with nuclear magnetic resonance spectroscopy (NMR), Fourier transform infrared (FT-IR) spectroscopy, and elemental analysis. Finally, a novel magnetic nanoadsorbent was synthesized by modification the surface of Fe_3O_4 nanoparticles by N^2,N^6-di(thiazol-2-yl)pyridine-2,6-dicarboxamide. The prepared magnetic nanoadsorbent was successfully used for removal of Zn^{2+} and Cd^{2+} ions from industrial wastes and the effects of the affecting parameters such as pH, possible interfering ions, contact time, concentration of target ions, background electrolytes and temperature were investigated. The maximum adsorption capacities of Zn^{2+} and Cd^{2+} were found to be 149.2 and 112.4 mg g^{-1}, respectively. The required times for quantitative removal of Zn^{2+} and Cd^{2+} were 30 and 45 min, respectively. Appropriate characteristics of the proposed nanoadsorbent such as high adsorption capacity, stability, reusability, easy synthesis and easy separation, make it suitable adsorbent for practical removal of Zn^{2+} and Cd^{2+} ions from industrial wastes.

***Keywords**:* Nanoadsorbent; Fe3O4; Magnetic; Heavy metal ion; Industrial waste

Abbreviations: BET; Brunauer–Emmett–Teller, DPD; N2,N6-di(thiazol-2-yl)pyridine-2,6-dicarboxamide, FAAS; Flame atomic absorption spectroscopy, FT-IR; Fourier transform infrared, MNP; magnetic nanoparticles, SEM; scanning electron microscopy, XRD; X-ray diffraction

1. Introduction

Among the different solid materials, composite materials due to their pre-designed structures have outstanding roles in multipurpose and complicated applications. Today, composite materials have widespread applications in industry and research. Some of their applications include detection and determination of chemical and biological species [1, 2], removal of toxic pollutants from industrial wastes

* Corresponding author. Tel.: +98 3133913287; fax: +98 3133912352. E-mail address: Kiomarszargoosh@cc.iut.ac.ir

and aqueous solutions [3-5], drug delivery for special tissues [6, 7] hyperthermia therapy [8], fabrication of fuel cells [9], designing of capacitors with high level of capabilities [10] and production of chemicals via inexpensive or safe routes [11, 12].

Among the different types of composite materials, magnetic nanoadsorbents have been proposed by several researchers for removal or isolation of pollutants from industrial wastes and environmental waters, because magnetic nanoadsorbents can be easily separated from solutions [13-15].

Magnetic iron oxides such as magnetite (Fe_3O_4), hematite (α- Fe_2O_3) and maghemite (γ- Fe_2O_3) have been frequently used for production of magnetic nanoadsorbent for treatment of polluted effluents. These iron-based nanoadsorbents have several advantages; they are cheap, reusable, easily accessible and environmentally friendly adsorbents. Specially, magnetite (Fe_3O_4) nanoparticles due to their high magnetic properties and high adsorption capacity have attracted special attentions [16]. In addition, in aqueous solutions the surface of the Fe_3O_4 nanoparticles is rich of hydroxyl groups. Presence of hydroxyl groups on the surface of the Fe_3O_4 nanoparticles provides excellent opportunities for surface modification of these nanoparticles. Surface modification of the Fe_3O_4 nanoparticles with suitable organic reagents can prevent the aggregate formation between nanoparticles and, hence enhance their adsorption capacity [17]. Furthermore, surface modification of the Fe_3O_4 nanoparticles can significantly improve the selectivity of this nanoadsorbent for adsorption of target pollutants via effective interaction between active sites of organic modifier and pollutant particles. For example, if the target pollutants are heavy metal ions, the active sites include the functional groups such as carboxyl, hydroxyl, amine, sulfide, thiol and amide [18, 19].

For removal of heavy metal ions from environmental waters or industrial wastes presence of large amounts of alkaline earth metal ions in the samples is serious challenge, because these ions can occupy the active sites of the modified nanoadsorbents and, hence reduce their ability for removal of toxic heavy metal ions from solution. Our previous works showed that surface modification of the Fe_3O_4 nanoparticles with suitable ligating agents can significantly reduce the interferences of alkaline/alkaline earth metal ions on the adsorption of heavy metal ions. These ligating agents must include soft donor atoms such as sulfur and nitrogen to form reversible complexes with heavy metal ions as soft acceptor atoms [16, 17]. In addition, these ligating agents must include suitable functional groups to be effectively immobilized on the surface of the Fe_3O_4 nanoparticles via covalent or hydrogen bonds.

However, there are some problems that limited the practical applicability of the magnetic nanoadsorbents for removal of toxic substances from real samples such as industrial wastes. For example, Fe_3O_4 nanoparticles must be covered with a shell of poly acrylic acid for additional modification. Solubility of poly acrylic acid in water introduces some degree of instability in the structure of magnetic nanoadsorbents. In addition, lack of selectivity can significantly reduce the adsorption capacity of the magnetic nanoadsorbents during treatment of real samples containing considerable amounts of different pollutants.

In this work, we report preparation of a stable and reusable magnetic nanoadsorbent for removal of Zn^{2+} and Cd^{2+} from industrial wastes in the presence of considerable amounts of coexisting cations. In this regard, in the first stage a novel ligating agent, N^2,N^6-di(thiazol-2-yl)pyridine-2,6-dicarboxamide, (DPD), was synthesized via reaction between 2-aminothiazole and 2,6- pyridinedicarboxylic acid in n-methylpyrrolidine. The obtained DPD was characterized with nuclear magnetic resonance spectroscopy (NMR), Fourier transform infrared (FT-IR) spectroscopy and elemental analysis. In the second stage, magnetic Fe_3O_4 nanoparticles were prepared via chemical coprecipitation method [20] and their size and distribution were studied using scanning electron microscopy (SEM). In the third stage, novel magnetic nanoadsorbent was synthesized by modification the surface of Fe_3O_4 nanoparticles by N^2,N^6-di(thiazol-2-yl)pyridine-2,6-dicarboxamide. It must be noted that the DPD not only includes nitrogen and sulfur atoms for interaction with Zn^{2+} and Cd^{2+} ions, but also includes carbonyl groups for direct immobilization of DPD on the Fe_3O_4 nanoparticles. Thus, poly acrylic acid was removed from modification steps, and hence the obtained magnetic Fe_3O_4@DPD nanoadsorbent is completely stable in water.

In the fourth stage, the prepared magnetic nanoadsorbent was successfully used for removal of Zn^{2+} and Cd^{2+} ions from industrial wastes and the effects of the affecting parameters such as pH, contact time, concentration of heavy metal ions, background electrolytes and temperature were investigated. Finally,

the adsorption kinetics and isotherms were used to investigate the mechanism of the adsorption of metal ions on the surface of the synthesized nanoadsorbent.

2. Materials and methods

2.1. Materials

All chemicals and reagents were analytical grade. Hydrochloric acid (HCl), sodium hydroxide (NaOH), iron(III) chloride ($FeCl_3 \cdot 6H_2O$), iron(II) chloride ($FeCl_2 \cdot 4H_2O$), cadmium chloride ($CdCl_2 \cdot 2.5H_2O$), zinc Cloride $ZnCl_2$ were purchased from Merck. 2-aminothiazole, 2,6- pyridinedicarboxylic and n-methylpyrrolidine, were purchased from Sigma-Aldrich. Doubly distilled deionized water was used throughout.

2.2 Apparatus

A Perkin-Elmer 2380-Waltham flame atomic absorption spectrometer (FAAS) was used for determination of the metal ions concentration. A Jenway (USA) model 3020 pH meter with a combined glass electrode was used after calibration against standard Merck buffers for pH determinations. A totally glass Fisons (UK) double distiller was used for preparation of doubly distilled water. Fourier transform infrared (FT-IR) spectra were obtained with a Bruker model Equinox 55 LS101 FT-IR spectrophotometer. X-ray diffraction (XRD) measurements were carried using a Siemens D-5000 X-ray diffractometer (Germany) with Cu Kα radiation. The reaction was occurred on a MISONIX ultrasonic liquid processor, XL-2000 SERIES. Ultrasonic irradiation was carried out with the horn probe of the ultrasonic immersed directly in the solution mixture with frequency 2.25×10^4 Hz and power 100 W. Field-emission scanning electron microscopy (FE-SEM) S-4160 Hitachi (Japan) was used to investigate the morphology and size distribution of the prepared nanoadsorbent. Quantachrome Autosorb-1 system was used for Low temperature N_2-adsorption measurements. Before N_2-adsorption measurements, samples were heated at 353K under vacuum for 3 h.

2.3. Synthesis of Fe_3O_4 magnetic nanoparticles (MNPs)

A previously reported method was used for preparation of Fe_3O_4 magnetic nanoparticles (MNPs) [20]. $FeCl_3$ (10.8 g) and $FeCl_2$ (4.0 g) were dissolved in 50 mL of HCl (2 mol L^{-1}). A vacuum pump was used for degassing of solution. Degassed solution was filled with N_2 gas. After sonication for 10 min, aqueous ammonia solution (28%, 80 mL) was slowly added to the mixture. The obtained Fe_3O_4 MNPs separated magnetically from solution and washed with 150 mL of deionized water. Then, Fe_3O_4 MNPs were washed 5 times with ethanol and dried under vacuum at 60 °C for 4 h.

2.4. Synthesis of N^2,N^6-di(thiazol-2-yl)pyridine-2,6-dicarboxamide(DPD)

A previously reported method for preparation of some polyhydrazides was used for synthesis of DPD [21]. Briefly, the 25 mL side-arm flask with a magnetic stirring bar was charged with 2-aminothiazole **a** (0.2 g, 2.0 mmol) and 2,6- pyridinedicarboxylic acid **b** (0.167 g, 1 mmol) and n-methylpyrrolidine (2 mL) as solvent (see Figure1). Then, the mixture was refluxed for 12 h at 90 °C. After removal of the solvent under reduced pressure, DPD was obtained as yellowish- white solid. The resulting DPD **c** was dried under nitrogen atmosphere and used in the next steps. The mass of the prepared DPD was 0.29 g (yield 88%).

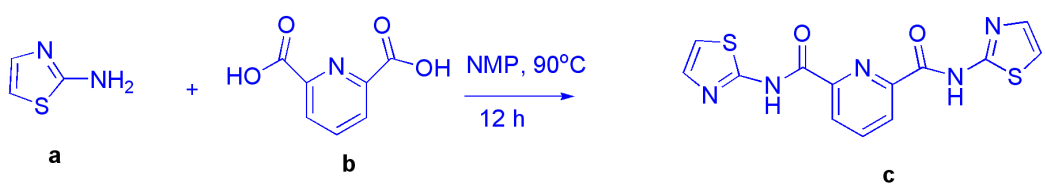

Figure 1. Synthesis of N^2,N^6-di(thiazol-2-yl)pyridine-2,6-dicarboxamide

2.5. Preparation of magnetic nanoadsorbent

Under nitrogen atmosphere, the Fe_3O_4 MNPs (0.2 g) were ultrasonicated for 30 min in 10 mL of water to obtain dispersed MNPs. Then, N^2,N^6-di(thiazol-2-yl)pyridine-2,6-dicarboxamide (0.66 g, 2 mmol) was

added to the dispersed Fe_3O_4 MNPs solution. The mixture was dispersed for 2 h by ultrasonication. Under ultrasonication, the temperature was slowly (during 20 min) raised to 50 °C and stirred for 28 h at this temperature. Then, resulting nanoadsorbent, Fe_3O_4@DPD, was magnetically separated from solution, washed with 100 mL of water and dried in vacuum at 50 °C. A possible mechanism for adsorption of Zn^{2+} and Cd^{2+} ions by the magnetic Fe_3O_4@DPD nanoadsorbent has been shown in Figure 2.

2.6 Adsorption Measurement

The adsorption characteristics of the prepared Fe_3O_4@DPD nanoadsorbent for Zn^{2+} and Cd^{2+} were studied in batch experiments. In these experiments the effects of different affecting parameters were investigated. The effects of pH (1.0–6.0), kinetics time (5–90 min), temperature (298-328 K) and adsorption isotherms (initial concentration 0.05-150 mg L^{-1}) of the studied metal ions were studied. In addition, the effects of possible interfering ions in real samples (such as alkaline/earth metal ion concentrations) in the concentration range of 0–0.3 mol L^{-1} were studied. In all experiments 0.020 g of Fe_3O_4@DPD nanoadsorbent adsorbent was added to a 50 mL of a target metal ion solution. The experiments were done at room temperature and the pH of the solutions was kept at a constant value during adsorption process. The required time for equilibrium establishment between adsorbent and metal ion solution was less than 1 h. After equilibrium establishment, the Fe_3O_4@DPD particles were magnetically separated from solution. To determine the amount of the metal ion adsorbed on the surface of the Fe_3O_4@DPD particles the remained concentration of the metal ion in the solution after equilibrium establishment was determined by flame atomic absorption spectroscopy. Equation 1 as a previously defined equation [16, 17] was used for calculation of the adsorbed mass (mg) of the metal ion per unit mass (g) of the Fe_3O_4@DPD adsorbent. Removal efficiencies (%Re) were calculated by using equation 2 [16, 17].

$$q_e = \frac{(C^0 - C_e) \times v}{m \times 1000} \quad \text{(eq 1)}$$

$$\%\,\mathrm{Re} = \frac{(C^0 - C_e)}{C^0} \times 100 \quad \text{(eq 2)}$$

In these equations C^0 and C_e are the concentrations (mg L^{-1}) of the metal ions in the solution before and after the adsorption process, respectively; *v* is the volume of the solution (mL) and m is the mass of the Fe_3O_4@DPD adsorbent used (g).

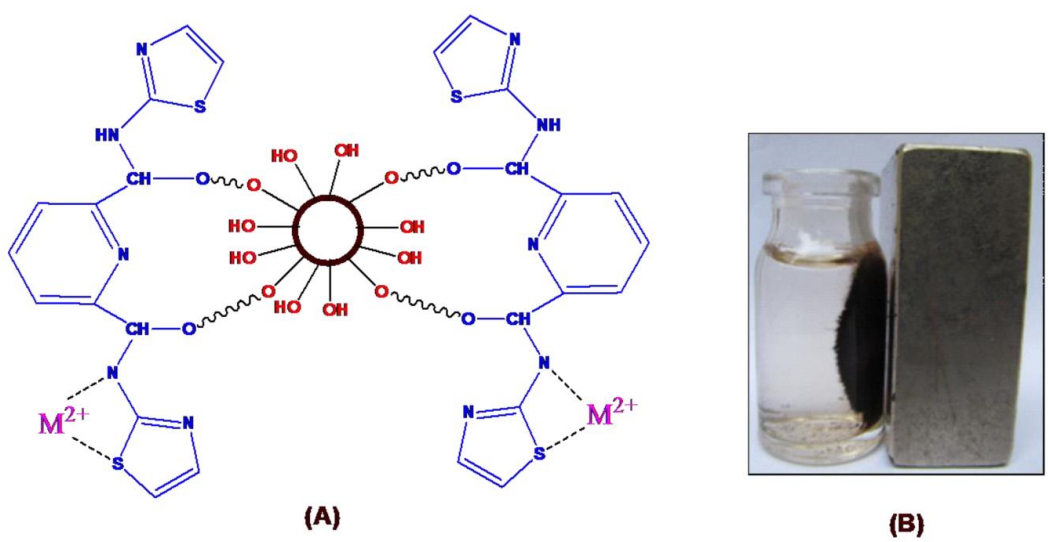

Figure 2. (A) Adsorption of M^{2+} ions by of magnetic Fe_3O_4@DPD nanoadsorbent, (B) separation of magnetic Fe_3O_4@DPD nanoadsorbent from solution.

2.7. Recovery and Reuse

To examine the possibility of the adsorbed metal ion recovery from the Fe_3O_4@DPD adsorbent 0.02 g of the metal ion loaded Fe_3O_4@DPD adsorbent were stirred with HCl solution at room temperature for 3 h. The volume and concentration of the HCl solution were 10 mL and 0.2 mol L^{-1}, respectively. Then, the leached metal ion concentration in the solution was determined by FAAS. Then, Fe_3O_4@DPD nanoadsorbent were neutralized by sodium hydroxide 0.1M and washed 10 times with deionized water and again used in adsorption processes to investigate the reusability of the recovered adsorbent. Each, Fe_3O_4@DPD adsorbent was used at least four times in the repeated adsorption−desorption cycles.

3. Results and discussion

3.1. Characterization of the prepared materials

Figure 3 shows the SEM images of the obtained Fe_3O_4 nanoparticles (A) and Fe_3O_4@DPD nanoadsorbent (B). As is clear from Figure 3 (A), the diameters of the Fe_3O_4 nanoparticles are about 10−35 nm. As can be seen from Figure 3 (B), the prepared Fe_3O_4@DPD nanoadsorbent has relatively uniform particles without notable aggregation. The specific surface area of the Fe_3O_4 particles and Fe_3O_4@DPD nanoadsorbent were 75.2 and 77.3 m^2 g^{-1}, respectively according to BET measurements. Higher surface area of the Fe_3O_4@DPD particles may be due to prohibition of aggregate formation between Fe_3O_4 particles by DPD organic shell.

The preparation of the Fe_3O_4@DPD nanoadsorbent was confirmed by FT-IR. The FT-IR spectra of the Fe_3O_4, N^2,N^6-di(thiazol-2-yl)pyridine-2,6-dicarboxamide (DPD) and Fe_3O_4 @DPD have been depicted in Figure 4a−c, respectively. As can be seen from Figure 4a, peaks of 500−750 cm^{-1} belong to the Fe_3O_4 as previously reported for Fe_3O_4 nanoparticles [22]. As is clear from Figure 4b, presence of a strong peak at 3274 cm^{-1} is ascribed to the stretching vibration of NH group. Presence of a strong peak at 3036 cm^{-1} is clearly representative of the aromatic CH bonds. Carbonyl bond of the amide functional group can be identified via its strong peak at 1756 cm^{-1}. In addition a strong bond at 1683 cm^{-1} is representative of the CN bonds of the pyridine moiety in the structure of the DPD. Finally, the similarity between Figure 4b,c spectra clearly confirms that DPD has been successfully bonded to the surface of Fe_3O_4 nanoparticles.

For further structural confirmation of DPD its ^{1}H-NMR spectrum in DMSO is shown in Figure 5. As is clear from Figure 5, peaks at 7.37, 7.63, 8.30, 8.39 and 13.37 are ascribed to protons of thiazol ring (no 4), thiazol ring (no. 5) pyridine ring (no. 3), pyridine ring (no. 2) and amide (no. 1) respectively. It is immediately obvious that there is a satisfactory agreement between the positions of the recorded ^{1}H-NMR peaks and the expected positions for protons of DPD. In addition, elemental analysis results showed that prepared DPD includes C (47.11%), N (20.91%), S (19.05%), O (10.20%) and H (2.73%). These results are in excellent agreement with calculated values for DPD: C (47.13%), N (21.15%), S (19.33%), O (9.67%) and H (2.72%). Furthermore, elemental analysis of the Fe_3O_4@DPD nanoadsorbent showed that each g of the nanoadsorbent includes 0.583 g of DPD.

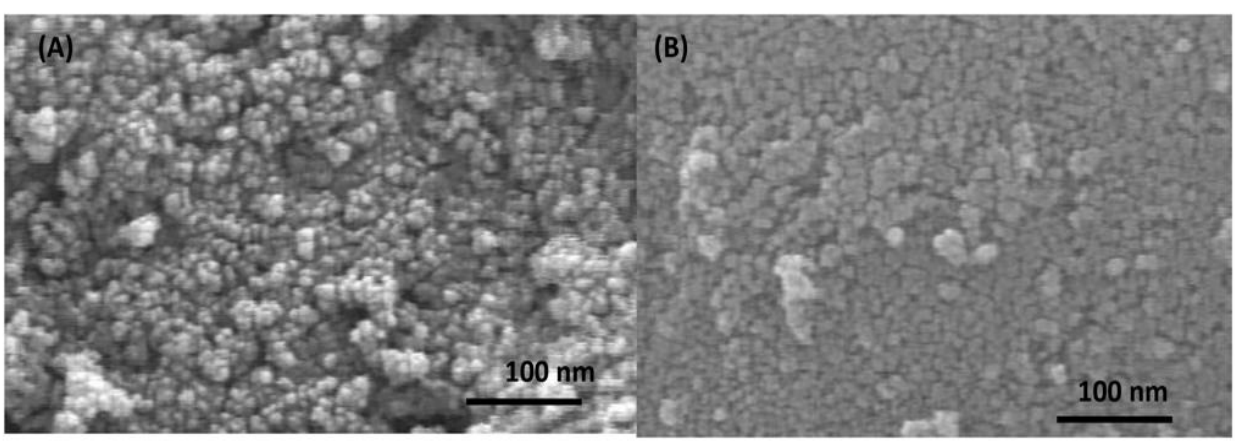

Figure 3. SEM image of the Fe_3O_4 MNPs (A) and Fe_3O_4@DPD nanoadsorbent (B).

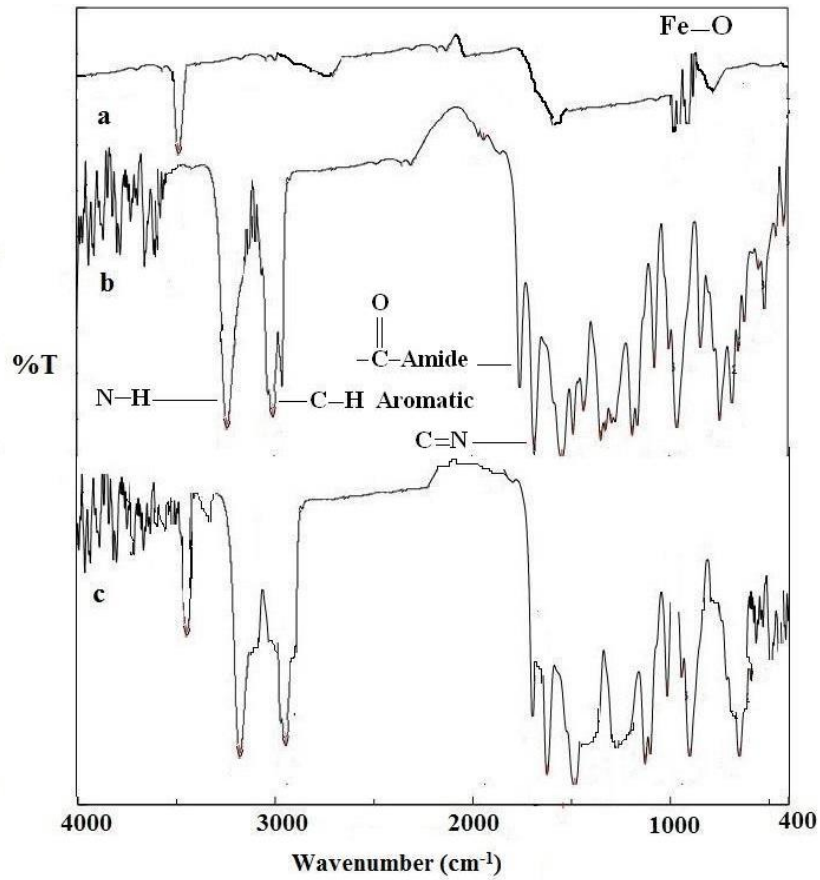

Figure 4. FT-IR spectra of Fe_3O_4 (a), DPD (b) and Fe_3O_4@DPD (c).

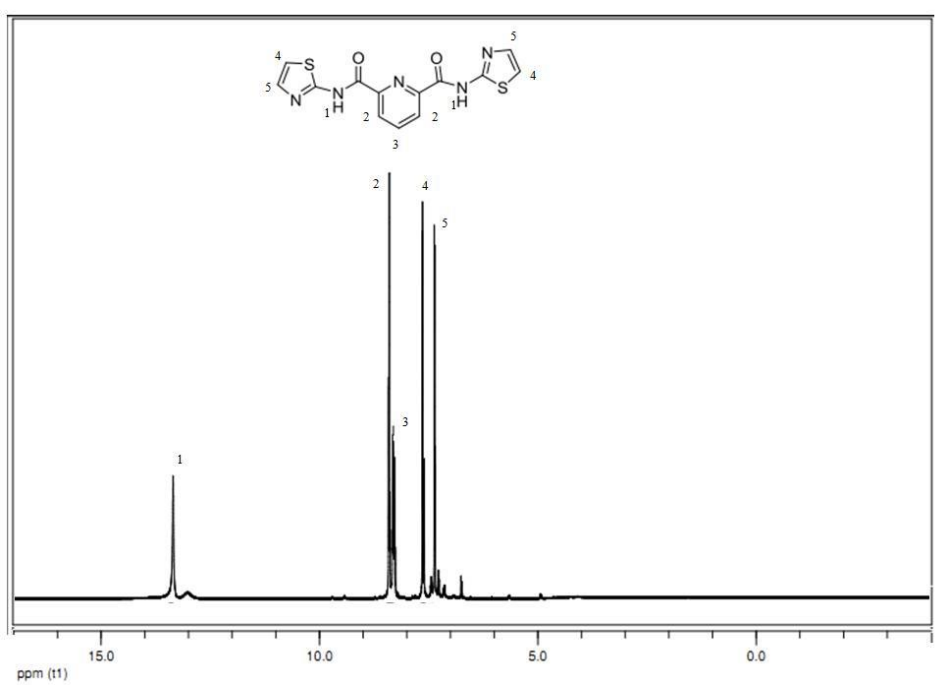

Figure 5. ^{1}H-NMR spectrum of DPD in DMSO.

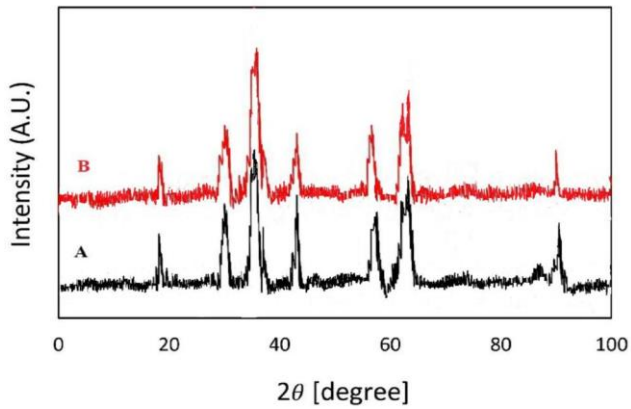

Figure 6. The XRD patterns of the synthesized Fe_3O_4 MNPs (a) and Fe_3O_4@DPD nanoadsorbent (b).

For phase confirmation of the prepared Fe_3O_4 nanoparticles the XRD patterns of the Fe_3O_4 MNPs and Fe_3O_4@DPD were recorded. The results are shown in Figure 6. The reflection peak positions and relative intensities of the MNPs are in well agreement with XRD patterns for Fe_3O_4 MNPs in the literature [18, 22]. No reflections for other impurities such as Fe_2O_3 are found in the pattern which further confirms that the synthesized Fe_3O_4 are pure. In addition, the XRD patterns of the Fe_3O_4 MNPs and Fe_3O_4@DPD nanoadsorbent have same peak positions, indicating that during nanoadsorbent preparation the phase of the Fe_3O_4 MNPs doesn't change.

3.2. Adsorption properties of the prepared Fe_3O_4@DPD nanoadsorbent for Zn^{2+} and Cd^{2+}.

3.2.1. Effect of pH

Adjusting the pH of the metal ion solutions has significant effect on the removal efficiency of the Fe_3O_4@DPD adsorbent for Zn^{2+} and Cd^{2+} ions, because at low pH values (lower than 4) protonation of the nitrogen and sulfur atoms of the active sites decreases the binding ability of the active sites toward metal ions. On the other hand, at pH values upper than 8, Zn^{2+} and Cd^{2+} may form hydroxide precipitates. Figure 7 demonstrates the influence of pH of test solution on the adsorption of Zn^{2+} and Cd^{2+} by Fe_3O_4@DPD nanoadsorbent at pH 1–6. As is clear from Figure 7, there are noteworthy increases in removal efficiency with increasing pH values of the test solution from 1 to about 5. At pH values upper than 5, the removal efficiency value of Zn^{2+} is approximately constant, while removal efficiency value of Cd^{2+}moderately increases. To achieve optimum removal efficiency and prevent the risk of the hydroxide precipitation of Zn^{2+} and Cd^{2+}, in the subsequent experiments, pH values of 5 and 6 were selected as optimum values for removal of Zn^{2+} and Cd^{2+}, respectively. The pH of the solutions was adjusted by the use of acetic acid/sodium acetate buffer. Industrial wastes (strongly acidic or basic solutions) were first neutralized with HCl or NaOH and then pH adjustments were accomplished by the use of acetic acid/sodium acetate buffer.

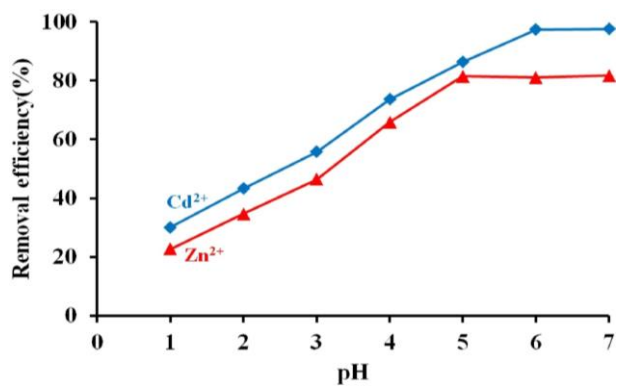

Figure 7. Effect of pH on the adsorption of Zn^{2+} and Cd^{2+}; adsorbent: 0.02 g, concentration of initial metal ions: 20 mg L^{-1}; volume of metal ions solution: 50 mL; time: 1 h, at 298 K.

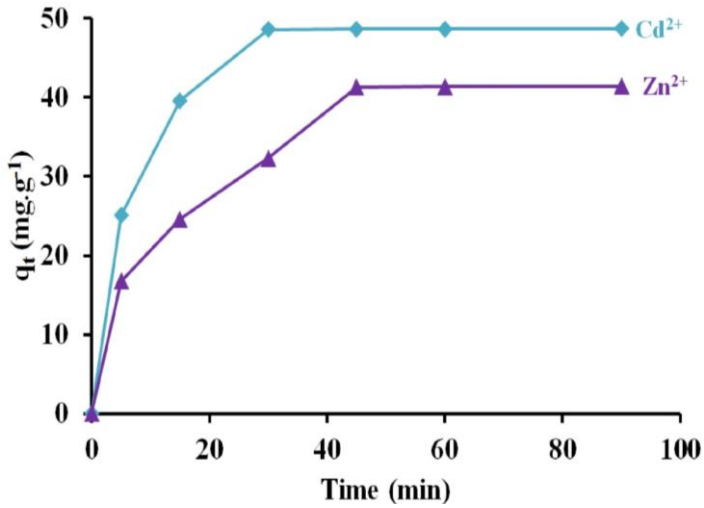

Figure 8. Effect of time on the adsorption of Zn^{2+} and Cd^{2+}; adsorbent: 0.02 g; concentration of metal ions: 20 mg L^{-1}; volume of test solution: 50 mL; pH: (5 for Zn^{2+} and 6 for Cd^{2+}); temperature: 298 K.

3.2.2. Adsorption kinetics

In practical point of view, adsorbents must have as high as possible adsorption rate to show usability in continuous systems. Figure 8 shows the effects of time on the adsorption of the Zn^{2+} and Cd^{2+} by the Fe_3O_4@DPD nanoadsorbent. As can be seen from Figure 8, the Cd^{2+} ions rapidly reached equilibrium in less than 30 min, while establishment of equilibrium for Zn^{2+} needs about 45 min. Compared with other reported adsorbents, the Fe_3O_4@DPD nanoadsorbent shows fast kinetics [23, 24]. This fast adsorption could be attributed to the larger surface area of Fe_3O_4@DPD adsorbent and the higher affinity of the nitrogen and sulfur active sites for complex formation with Zn^{2+} and Cd^{2+}.

Lagergren pseudo-first-order (eq 3) and pseudo-second-order (eq 4) models [25] were used for further studying of the adsorption kinetics of Zn^{2+} and $Cd^{2+}$with Fe_3O_4@DPD adsorbent:

$$\ln(q_e - q_t) = \ln(q_e) - k_1 t \qquad \text{(eq 3)}$$

$$\frac{t}{q_t} = \left(\frac{1}{q_e}\right)t + \left(\frac{1}{k_2 \times q_e^{\,2}}\right) \qquad \text{(eq 4)}$$

In these equations q_t (mg g^{-1}) demonstrates the adsorption at time t (min); q_e (mg g^{-1}) shows the adsorption capacity at equilibrium time; k_1 (min^{-1}) is the rate constant for the pseudo-first-order model and k_2 (g mg^{-1} min^{-1}) is the rate constant for the pseudo-second-order model. The kinetic adsorption data were fitted to equation (3) and (4), and the obtained results were shown in Figure 9 and Table 1. As can be seen from Table 1, the correlation coefficient (R) for the second-order kinetic model is about unity (0.99) which confirms the second-order nature of the adsorption of Zn^{2+} and Cd^{2+}on the Fe_3O_4@DPD adsorbent. This observation is in agreement with the complexation mechanism proposed in Figure 2 for adsorption of Zn^{2+} and Cd^{2+} on the surface of Fe_3O_4@DPD adsorbent [26].

Table 1. Characteristics of the applied kinetics models for adsorption of Cd^{2+} and Zn^{2+} by DPD@Fe_3O_4 nanoadsorbent.

Metal ions	2nd order			1st order			q (mg g^{-1}) [a]
	R^2	q_e (mg g^{-1})	k_2	R^2	q_e (mg g^{-1})	k_1	
Cd^{2+}	0.9997	51.6±2.0	0.0040	0.8317	18.1 ± 4.3	0.0776	48.8 ± 2.2
Zn^{2+}	0.9994	46.1 ± 2.5	0.0029	0.8828	30.8 ± 7.4	0.0771	42.5 ± 1.8

[a] $q\ (mg\ g^{-1}) = q_{experimental}$

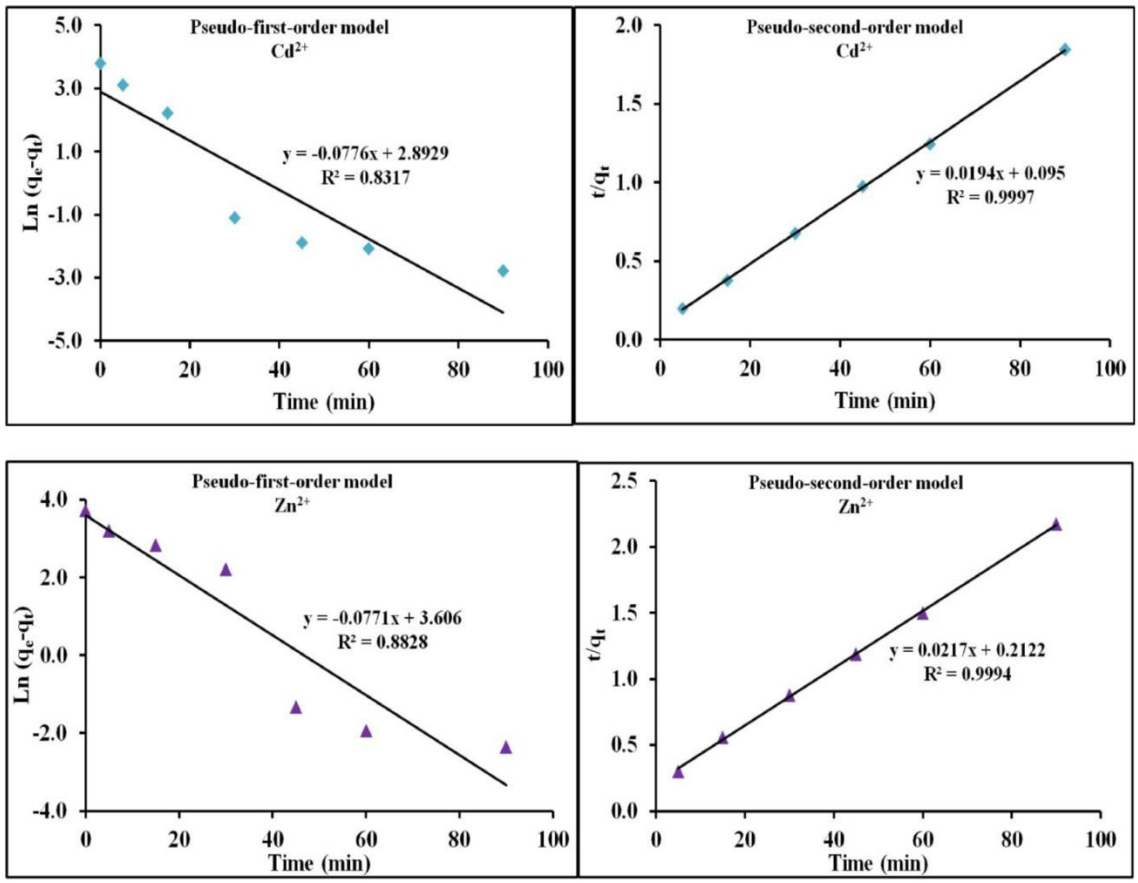

Figure 9. Fitting of the experimental results in Lagergren pseudo-first-order and pseudo-second-order models

3.2.3. Adsorption isotherms of Fe_3O_4@DPD adsorbent for Zn^{2+} and Cd^{2+}.

Generally, the adsorption capacities of the adsorbents depend on the concentration of the adsorbate in solution, thus the effects of the solution concentration on the adsorption capacities of the Zn^{2+} and Cd^{2+} were investigated at optimum pH values (5 for Zn^{2+} and 6 for Cd^{2+}) and temperature 298 K. The mass of the Fe_3O_4@DPD adsorbent was 0.020 g and the concentration ranges were 0.5–150 and 5–150 mg L^{-1} for Zn^{2+} and Cd^{2+}, respectively. The contact times for Zn^{2+} and Cd^{2+} were 45 and 30 min, respectively. After equilibrium establishment between Fe_3O_4@DPD adsorbent and metal ion solution, the remained concentration of the metal ion in the solution was determined by using FAAS. Langmuir model (eq 5) and Freundlich model (eq 6) were used for analysis the equilibrium isotherms for the adsorption of the Zn^{2+} and Cd^{2+} ions on the surface of the Fe_3O_4@DPD adsorbent:

$$\frac{C_e}{q_e} = \left(\frac{1}{q_{max}}\right) C_e + \left(\frac{1}{K_L \times q_{max}}\right) \quad \text{(eq 5)}$$

$$q_e = K_F \times C_e^{(1/n)} \quad \text{(eq 6)}$$

In these equations, q_e, C_e, q_m, K_L, K_F and n are the equilibrium adsorption capacity of ions on the adsorbent (mg g^{-1}), the equilibrium ions concentration in solution (mg L^{-1}), the maximum capacity of the adsorbent (mg g^{-1}), the Langmuir adsorption constant (L mg^{-1}), the Freundlich constant (L mg^{-1}) and the heterogeneity factor, respectively [27].

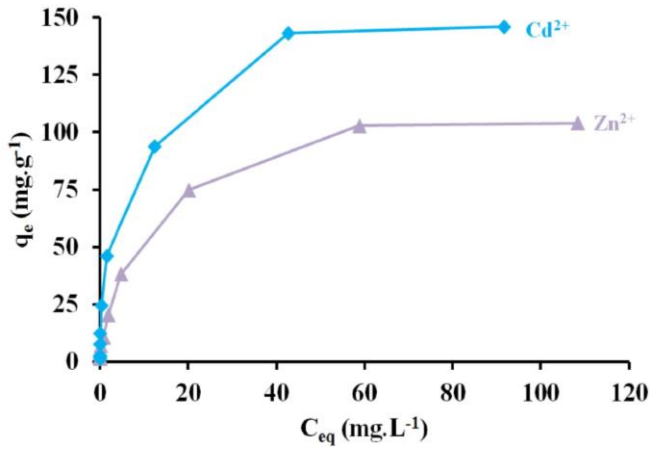

Figure 10. Equilibrium isotherms of Zn^{2+} and Cd^{2+} by Fe_3O_4@DPD nanoadsorbent, performed in batch mode; adsorbent: 0.02 g, initial concentration of metal ions: (0.5–150 mg L^{-1} for Zn^{2+} and 5–150 mg L^{-1} for Cd^{2+}); temperature: 298 K; pH: (5 for Zn^{2+} and 6 for Cd^{2+}); time: (30 min for Cd^{2+} and 45 min for Zn^{2+}).

The results were depicted in Figure 10, Figure 11 and Table 2. As is obvious from Figure 10, Figure 11 and Table 2, the equilibrium capacities (q_e) of the Zn^{2+} and Cd^{2+} show remarkable enhancement with increasing the concentration of Zn^{2+} and Cd^{2+} in solution until reaching equilibrium. Furthermore, correlation coefficients (R) values for Langmuir model are higher than those of the Freundlich model. These results indicate that adsorption isotherm data for $Zn^{2+}$and Cd^{2+} are clearly in better agreement with Langmuir model rather than Freundlich model. Appropriate fitness of the experimental results to Langmuir model indicates that Zn^{2+} and Cd^{2+} ions have been adsorbed as monolayer on the surface of the adsorbent particles. Again, this observation confirms our proposed mechanism for adsorption of Zn^{2+} and Cd^{2+} ions onto the Fe_3O_4@DPD particles via complex formation with donor sites of the DPD. As can be seen from Table 2, the maximum capacity (q_m) for Cd^{2+} and Zn^{2+} calculated by the Langmuir equation are 149.2 and 112.4 mg g^{-1}mg g^{-1}, respectively. The observed differences in the maximum capacities of Zn^{2+} and Cd^{2+} are most probably due to their different ability to interact with active sites of the Fe_3O_4@DPD adsorbent surface; Cd^{2+} ions have lower solvation energy than Zn^{2+} ions, thus they can more easily be released from solvent cages and interact with active sites of adsorbent. In addition, Cd^{2+} ions are softer acceptor than Zn^{2+} ions, thus, they have stronger interactions with soft donor sites (sulfur and nitrogen atoms) of the nanoadsorbent.

Intrinsic ability of the Fe_3O_4 nanoparticles for adsorption of heavy metal ions has been reported in the literature [16]. To investigate the effects of the DPD modification on the removal performance of the prepared Fe_3O_4@DPD adsorbent, the adsorption capacity of the pristine Fe_3O_4 nanoparticles was measured under optimum conditions. The maximum adsorption capacities of the pristine Fe_3O_4 nanoparticles for Cd^{2+} and Zn^{2+} were 8.4 and 5.1 mg g^{-1}mg g^{-1}, respectively. As depicted in Table 2, the maximum adsorption capacities of the Fe_3O_4@DPD nanoadsorbent for Cd^{2+} and Zn^{2+} were 149.2 and 112.4 mg g^{-1}mg g^{-1}, respectively. These results indicate that the main adsorption of Cd^{2+} and Zn^{2+} takes place via interactions with DPD functional groups.

Table 2. Langmuir and Freundlich adsorption isotherm constants, correlation coefficients, and adsorption capacities (DPD@Fe_3O_4)

Metal ions	Langmuir			Freundlich		
	K_L (L mg^{-1})	q_m (mg g^{-1})	R^2	K_F ($mg^{1-(1/n)}$ $L^{1/n}$ g^{-1})	n	R^2
Cd^{2+}	0.510	149.2	0.9993	36.02	2.78	0.8724
Zn^{2+}	0.120	112.4	0.9997	12.71	1.94	0.8858

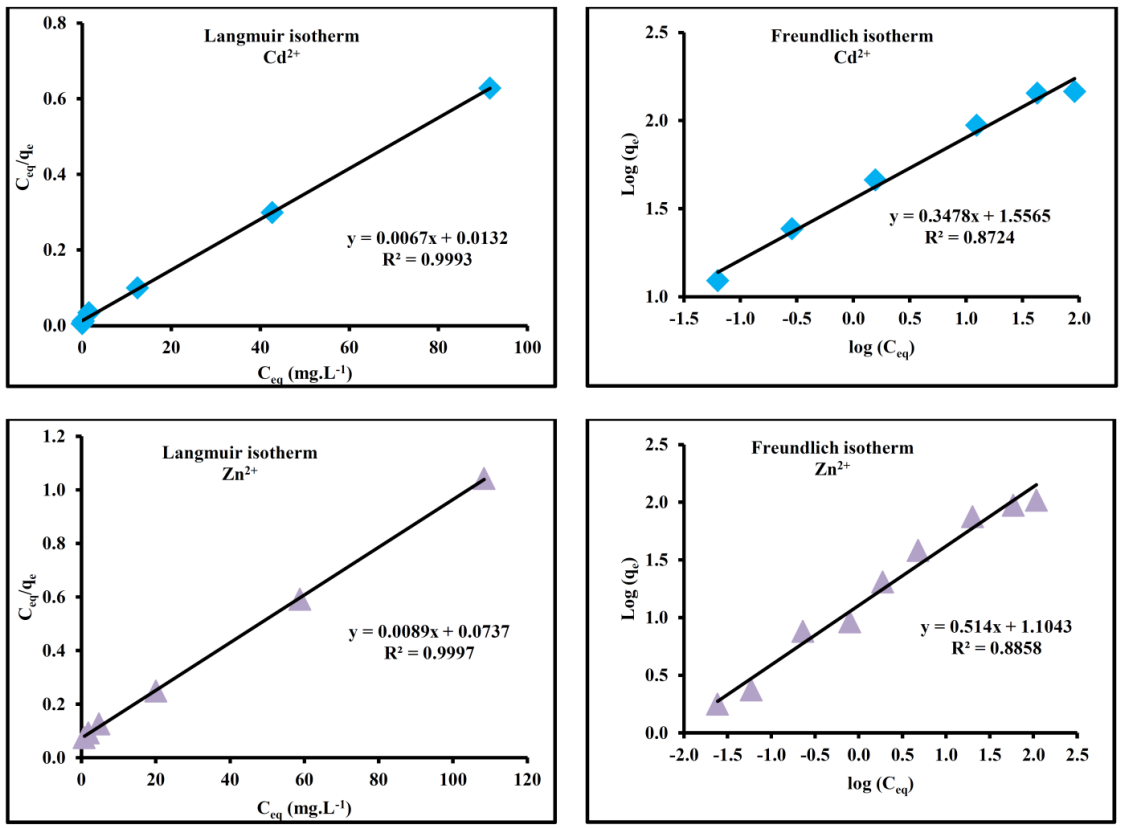

Figure 11. Fitting of the experimental results in Langmuir and Freundlich adsorption models.

Real samples such as industrial wastes include not only target pollutants but also possible interfering species, thus suitable adsorbents must be able to remove the target pollutants in the presence of coexisting interfering species. To examine the adsorptions characteristics of the target ions in the presence of possible interfering cations mixture of Zn^{2+} and Cd^{2+}, ions, 0.020 g Fe_3O_4@DPD adsorbent was added to a solution (50 mL) containing equal initial concentrations (20 mg L^{-1}) of Zn^{2+}, Cd^{2+}, Pb^{2+}, Hg^{2+}, Cu^{2+}, Ni^{2+}, Fe^{3+} and Al^{3+} ions. The pH of the solution was kept at 5.2 and the equilibrium time was selected as 60 min. After 60 min the adsorbent particles were separated by powerful magnets and the removal efficiencies *(%Re)* were calculated by using the equation 2. The obtained removal efficiencies for Zn^{2+} and Cd^{2+} were 71.1% and 84.2%, respectively. The removal efficiencies of other cations were less than 12 %. These results confirm the selectivity of the proposed adsorbent for removal of Zn^{2+} and Cd^{2+} in the presence of other coexisting metal cations.

To study the long term stability of the synthesized Fe_3O_4@DPD nanoadsorbent the maximum adsorption capacity of the fresh Fe_3O_4@DPD was compared with the maximum adsorption capacity of the 6 months old Fe_3O_4@DPD. It was found that the maximum adsorption capacity of the modified Fe_3O_4@DPD remains almost constant (112.4 ± 5.3 mg g^{-1} for Zn^{2+} and 149.2 ± 7.1 mg g^{-1} for Cd^{2+}) after 6 months. This observation confirms that, the prepared Fe_3O_4@DPD saves its ion adsorption ability during 6 months.

Table 3 compares the performance characteristics of the prepared Fe_3O_4@DPD adsorbent with some of the previously reported adsorbents for removal of Zn^{2+} and Cd^{2+} in the literature. As can be seen from Table 3, Fe_3O_4@DPD adsorbent shows remarkable enhancement in adsorption capacity for removal of Zn^{2+} and Cd^{2+}. High adsorption capacity of the prepared Fe_3O_4@DPD adsorbent together with other suitable characteristics such as reusability, easy synthesis and easy separation make it attractive adsorbent for removal of Zn^{2+} and Cd^{2+} from real samples such as industrial wastes and environmental waters.

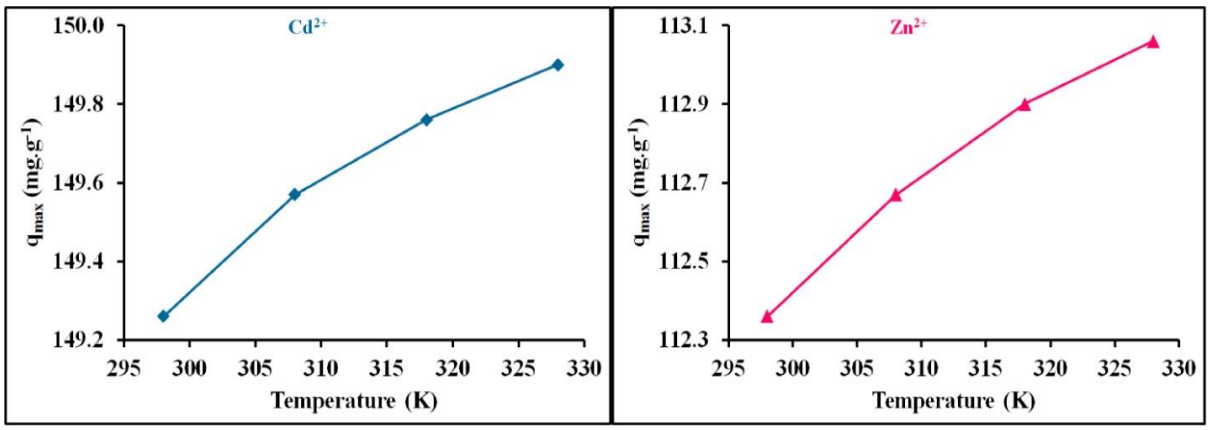

Figure 12. Effects of temperature on the maximum adsorption capacity (q_m) of the Fe_3O_4@DPD nanoadsorbent for adsorption of Zn^{2+} and Cd^{2+}, performed in batch mode; adsorbent: 0.02 g, initial concentration of metal ions: (0.5–150 mg L^{-1} for Zn^{2+} and 5–150 mg L^{-1} for Cd^{2+}); pH: (5 for Zn^{2+} and 6 for Cd^{2+}); time: time: (30 min for Cd^{2+} and 45 min for Zn^{2+}).

Table 3. Comparison of adsorption capacities of different adsorbents for removal of Cd^{2+} and Zn^{2+}.

Type of adsorbent	Adsorption capacities (mg g^{-1})		Reference
	Cd^{2+}	Zn^{2+}	
Polymer-modified Fe_3O_4 nanoparticles	29.6	43.4	[28]
TiO_2 nanoparticles	7.9	15.3	[29]
Silica-supported dithiocarbamate	40.3	-	[30]
Salicylic acid type chelate adsorbent	86.9	31.2	[31]
Fe_3O_4@PAA@TSH	107.5	51.3	[32]
Carbon nanotubes	10.86	-	[33]
Fe_3O_4@DPD	149.2	112.4	This work

3.2.4. Effect of temperature on the adsorption of Zn^{2+} and Cd^{2+}

To obtain proper removal efficiency some of the adsorbents must be used at special or limited range of temperature, this requirement impose additional costs with special apparatus for maintaining temperature at a pre-defined level. The effects of the temperature on the adsorption capacities of Zn^{2+} and Cd^{2+} were studied under batch condition at optimum pH (5 for Zn^{2+} and 6 for Cd^{2+}) and time (30 min for $Cd^{2+}$and 45 min for Zn^{2+}). These experiments were carried out in four different temperatures (298, 308, 318 and 328k). The mass of the Fe_3O_4@DPD adsorbent was 0.020 g and the concentration ranges were 0.5–150 and 5–150 mg L^{-1} for Zn^{2+} and Cd^{2+}, respectively. After equilibrium establishment between Fe_3O_4@DPD adsorbent and metal ion solution, the remained concentration of the metal ion in the solution was determined by using FAAS. Langmuir equation was used for calculation of the q_m values for each metal ion at each temperature. The results are shown in Figure 12. As is obvious, increasing temperature until a temperature of 328 K revealed no notable effect on the q_m values. This observation indicates that adsorption of Zn^{2+} and Cd^{2+} ions on the surface of the Fe_3O_4@DPD adsorbent includes no considerable changes in enthalpy. In Practical view, Freedom of temperature changes is significant advantage for an adsorbent, because samples can be treated without any temperature adjustments and, hence, the proposed method doesn't need special apparatus for controlling the temperature.

3.2.5. Effect of background electrolytes

Usually, real samples such as industrial wastes and environmental waters have complex matrixes, for example, groundwater and environmental samples often include considerable amounts of alkaline earth metal ions [29]. Thus, a suitable adsorbent must be able to remove heavy metal ions from samples in the

presence of an excess of alkaline/earth metal ions. To investigate the applicability of the prepared Fe_3O_4@DPD adsorbent for removal of target ions from real samples, the effects of the Na^+, K^+, and Mg^{2+} ions on adsorption capacity of Zn^{2+} were explored. As is obvious from Figure 13, the adsorption capacity of Zn^{2+} inconsiderably decreased (less than 4%) with addition alkaline/earth metal ions in a concentration range from 0.0 to 0.3 mol L^{-1}. The obtained results display that the proposed Fe_3O_4@DPD adsorbent can suitably remove Zn^{2+} and Cd^{2+} ions from solution in the presence of considerable concentration of alkaline/earth metal ions. Again, the observed results confirms our proposed mechanism for removal of Zn^{2+} and Cd^{2+} via complex formation with the donor sites of the DPD, accordingly Na^+, K^+, and Mg^{2+} cannot form complex species with DPD active sites and, hence, cannot be adsorbed on the Fe_3O_4@DPD adsorbent particles.

3.3. Desorption and repeated use

In practical applications, regeneration of adsorbents is an important issue, because can significantly reduce the cost of operations. Thus, the reusability of the prepared Fe_3O_4@DPD adsorbent was examined using the method described in Section 2.9, and the obtained results are shown in Figure 14. As can be seen, the adsorption capacity of Fe_3O_4@DPD adsorbent for removal of Zn^{2+} and Cd^{2+} is approximately constant for the 4 cycles, which shows that the complexation reaction between active sites of the Fe_3O_4@DPD adsorbent and Zn^{2+} and Cd^{2+} ions is reversible. Reversibility of the adsorption reaction makes it possible to reuse the same Fe_3O_4@DPD adsorbent for several time for removal of $Zn^{2+}$and Cd^{2+} from solution and, hence, reduce the overall cost of sample treatment.

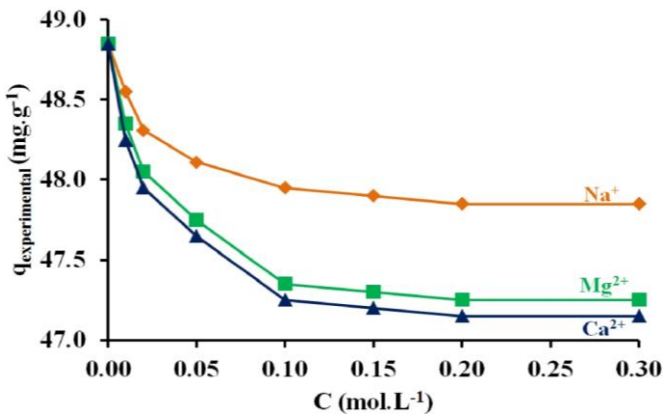

Figure 13. Effect of the alkaline/earth ions on the adsorption capacity of Fe_3O_4@DPD adsorbent for Zn^{2+}.

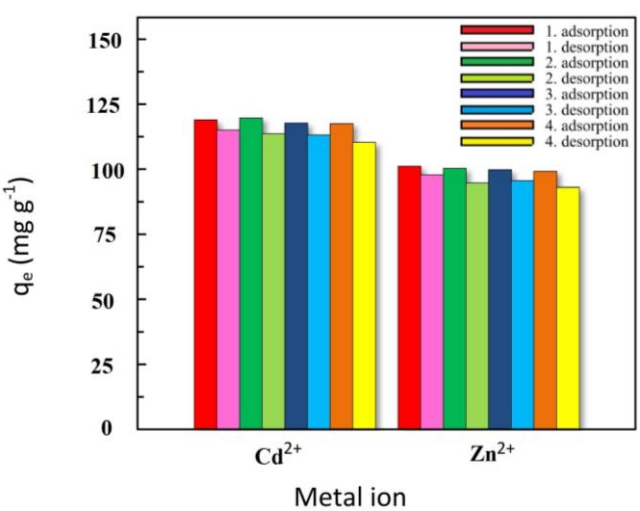

Figure 14. Performance of Fe_3O_4@DPD adsorbent by multiple regeneration cycles.

Table 4. Performance characteristics of the DPD@Fe_3O_4 adsorbent for removal of Zn^{2+} and Cd^{2+} from industrial wastes

Metal ions [a]	Hesam paint company		Moham industrial complex	
	Re %	C^0 (mg L^{-1})	Re %	C^0 (mg L^{-1})
Cd^{2+}	95.7 ± 3.6	175.8 ± 9.8	97.8± 3.62	0.7 ± 0.1
Zn^{2+}	78.8 ± 5.3	876.2±18.1	79.4 ± 4.53	423.4 ± 13.3

[a] Due to high concentrations of Cd^{2+} and Zn^{2+} in real samples the adsorption−desorption cycles were repeated

3.4. Removal of Zn^{2+} and Cd^{2+} from industrial wastes

The practical utility of the prepared nanoadsorbent for removal of Zn^{2+} and Cd^{2+} ions from real samples was evaluated using two different industrial wastes. Industrial wastes were collected (on June 2014) from Moham industrial complex (Iran, Isfahan) and Hesam paint producer company (Iran, Garmsar). The initial concentrations of Zn^{2+} and Cd^{2+} ions in the real samples were determined using a standard addition method and AAS detection. The remained concentration of Zn^{2+} and Cd^{2+} ions in the sample after treatment with adsorbent was determined AAS. The results were depicted in Table 4. Based on the obtained results the Fe_3O_4@DPD adsorbent is able to quantitatively remove the Zn^{2+} and Cd^{2+} ions from real samples.

4. Conclusion

A novel magnetic nanoadsorbent was synthesized by surface modification of Fe_3O_4 nanoparticles with N^2,N^6-di(thiazol-2-yl)pyridine-2,6-dicarboxamide.The synthesized Fe_3O_4@DPD nanoadsorbent was characterized using SEM, FT-IR, NMR, BET, and elemental analysis. The prepared magnetic nanoadsorbent was successfully used for removal of Zn^{2+} and Cd^{2+} ions from industrial wastes and the effects of the affecting parameters such as pH, contact time, concentration of heavy metal ions, background electrolytes, and temperature were investigated. The maximum adsorption capacities of Zn^{2+} and Cd^{2+} were found to be 112.4 and 149.2 mg g^{-1}, respectively. Appropriate characteristics of the proposed Fe_3O_4@DPD nanoadsorbent such as high adsorption capacity, stability, reusability, easy synthesis and easy separation, make it suitable adsorbent for practical removal of Zn^{2+} and Cd^{2+} from aqueous samples.

5. Acknowledgements

This work was financed by Isfahan University of Technology. The authors have declared no conflict of interest.

6. References

[1] M. Arvand, M. Hassannezhad, *Mater. Sci. Eng., C* 2014, *36*, 160–167.
[2] M. Baghayeri, E. Nazarzadeh Zare, M. M. Lakouraj, *Biosens. Bioelectron.* 2014, *55*, 259–265.
[3] A. Afkhami, S. Sayari, R. Moosavi, T. Madrakian, *J. Ind. Eng. Chem.* 2015, *21*, 920-924.
[4] Z. Qiang , X. Bao, W. Ben, *Water Res.* 2013, *47(12)*, 4107 –4114.
[5] S. Bakhshayesh, H. Dehghani, *Mater. Res. Bull.* 2013, *48 (7)*, 2614–2624.
[6] J. O. Mangual, S. Li, H. J. Ploehn, A. D. Ebner, J. A. Ritter, *J. Magn. Magn. Mater.* 2010, *322 (20)*, 3094-3100.
[7] G. Rezanejade Bardajee, Z. Hooshyar, M. Jahanbakhsh Asli, F. Emamjome Shahidi, N. Dianatnejad, *Mater. Sci. Eng.* C 2014, *36*, 277-286.
[8] P. B. Shete, R. M. Patil, N. D. Thorat, A. Prasad, R. S. Ningthoujam, S. J. Ghosh, S. H. Pawar, *Appl. Surf. Sci.* 2014, *288*, 149-157.
[9] N. Hasanabadi, S. R. Ghaffarian, M. M. Hasani-Sadrabadi, *Int. J. Hydrogen Energy* 2011, *36 (23)*, 15323-15332.
[10] D. Gui, C. Liu, F. Chen, J. Liu, *Appl. Surf. Sci.* 2014, *307*, 172-177.
[11] F. Zamani, S. M. Hosseini, *Catal. Commun.* 2014, *43*, 164-168.
[12] F. Zamani, S. Kianpour, *Catal. Commun.* 2014, *45*, 1-6.
[13] H. Bagheri, A. Roostaie, M. Y. Baktash, *Anal. Chim. Acta* 2014, *816*, 1-7.
[14] M. A. Salam, R. M. El-Shishtawy, A. Y. Obaid, *J. Ind. Eng. Chem.* 2014, *20 (5)*, 3559-3567.
[15] P. Xu, G. M. Zeng, D. L. Huang, C. L. Feng, S. Hu, M. H. Zhao, C. La, *Sci. Total Environ.* 2012*, 424*, 1-10.

[16] K. Zargoosh, H. Abedini, A. Abdolmaleki, M. R. Molavian, *Ind. Eng. Chem. Res.* 2013, *52*, 14944–14954.
[17] K. Zargoosh, H. Zilouei, M. R. Mohammadi, H. Abedini, *Clean – Soil, Air, Water* 2014, *42 (9999)*, 1–8.
[18] S. H. Huang, D. H. Chen, *J. Hazard. Mater.* 2009, *163*, 174-179.
[19] X. Liang, Y. Xu, G. Sun, L. Wang, Y. Sun, X. Qin, *Colloids Surf. A* 2009, *349*, 61-68.
[20] W. J. Chen, P. J. Tsai, Y. C. Chen, *Anal. Chem.* 2008, *80 (24)*, 9612-9621.
[21] A. abdolmaleki, *Iran. Polym. J.* 2007, *16 (11)*, 741-751.
[22] F. Ge, M. M. Li, H. Ye, B. X. Zhao, *J. Hazard. Mater.* 2012, *211–212*, 366-372.
[23] I. F. Nata, G. W. Salim, C. K. Lee, *J. Hazard. Mater.* 2010, *183*, 853-858.
[24] Q. Peng, Y. Liu, G. Zeng, W. Xu, C. Yang, J. Zhang, *J. Hazard. Mater.* 2010, *177 (1)*, 676-682.
[25] Y. M. Hao, M. Chen, Z. Hu, *J. Hazard. Mater*. 2010, *184*, 392-399.
[26] S. A. Nabi, M. Shahadat, A. H. Shalla, A. M. T. Khan, *Clean–Soil Air Water*2011, *39*, 1120-1128.
[27] K. Shin, J. Hong, J. Jang, *J. Hazard. Mater.* 2011, *190*, 36-44.
[28] A. R. Mahdavian, M. A. S. Mirrahimi, *Chem. Eng. J.* 2010, *159 (1)*, 264-271.
[29] J. Wang, S. Zheng, Y. Shao, J. Liu, Z. Xu, D. Zhu, *J. Colloid Interf. Sci.* 2010, *349(1)*, 293-299.
[30] E. Borai, E. El-Sofany, T. Morcos, *Adsorption* 2007, *13 (2)*, 95-104.
[31] P. Liang, T. Shi, J. Li, *Int. J. Environ. Anal. Chem.* 2004, *84*, 315-321.
[32] F. An, B. Gao, X. Dai, *J. Hazard. Mater.* 2011, *192*, 956-962.
[33] Y. H. Li, J. Ding, Z. Luan, Z. Di, Y. Zhu, C. Xu, B. Wei, *Carbon*, 2003, *41(14)*, 2787-2792.